Quantum-Chemical and Force-Field Investigations of Ice Ih: Computation of Proton-Ordered Structures and Prediction of Their Lattice Energies

Tomas K. Hirsch[†] **and Lars Ojamäe***[,‡]

Physical Chemistry, Arrhenius Laboratory, Stockholm University, SE-106 91 Stockholm, Sweden, and Department of Chemistry, IFM, Linköping University, SE-581 83 Linköping, Sweden

Received: April 8, 2004; In Final Form: July 18, 2004

The different possible proton-ordered structures of ice Ih for an orthorombic unit cell with 8 water molecules were derived. The number of unique structures was found to be 16. The crystallographic coordinates of these are reported. The energetics of the different polymorphs were investigated by quantum-mechanical density-functional theory calculations and for comparison by molecular-mechanics analytical potential models. The polymorphs were found to be close in energy, i.e., within approximately 0.25 kcal/mol H_2O, on the basis of the quantum-chemical DFT methods. At 277 K, the different energy levels are about evenly populated, but at a lower temperature, a transition to an ordered form is expected. This form was found to agree with the ice phase XI. The difference in lattice energies among the polymorphs was rationalized in terms of structural characteristics. The most important parameters to determine the lattice energies were found to be the distributions of water dimer H-bonded pair conformations, in an intricate manner.

I. Introduction

Ordinary ice, the hexagonal ice phase ice Ih, is proton-disordered at ordinary temperatures.[1−3] This means that although the oxygen framework exhibits long-range order and symmetry properties, no order at longer distances exist for which nearest-neighbor oxygens a water molecule donates its H-bonds to. However, at sufficiently low temperatures a proton-ordered phase has been found, ice XI.[4−9] The proton order−disorder transition temperature in KOH-doped ice Ih has been measured to be 72 K.[4,5] The transition temperature has also been suggested to occur at 237 K on the basis of Raman spectroscopy of samples of ice cores from Antarctica,[10] but similar experiments[11] as well as recent neutron diffraction studies[12] did not confirm those results.

To understand the nature of the ice XI−ice Ih transition, one needs to have a firm grasp of the energetics of the occurring H-bond arrangements in ice Ih. Several theoretical studies have been performed to elucidate the stabilities and properties of ice Ih structures.[13−27]

There are three purposes of this work. The first purpose is to investigate the properties of different ice polymorphs, with special emphasis on how the H-bond network affects the lattice energies of the different polymorphs. In this context, we try to identify structural characteristics that determine the relative stabilities of the polymorphs. We also point out the relations that do *not* hold in the solid state environment, when all factors (for example, complete geometry optimization) are accounted for. To achieve this goal, the main tool employed is first-principles quantum-chemical (QC) calculations to obtain accurate structures and energies. We thereby find it necessary to perform the calculations very carefully to enable the estimation of energy differences of a magnitude less than a few tenth's of a kcal/mol.

The second purpose is to compare the merits of quantum-chemical methods vis a vis force-field modeling using molecular-mechamics (MM) techniques. We judge whether force fields are accurate enough to reflect the subtle differences in structures and energies of different H-bond networks in the solid state.

The third purpose may actually be the most important one: to provide structures of different ice polymorphs, that in the future may be used as benchmark structures for different quantum-chemical or force field methods. For our first two purposes, a rather simple model system is satisfactory: we study all H-bond networks that can be constructed from an eight-molecule orthorombic unit cell of ice Ih. This system has previously been studied by Howe[16] where a scheme for obtaining different networks is reported. In the present study we derive and give the cell dimensions and the coordinates of the 16 unique structures.

This paper is organized as follows: Section II describes the methods used, both concerning the derivation of the different possible symmetry-unique structures of an 8-molecule ice Ih cell, as well as the computational quantum-chemical and force field methods employed. The computational results are shown in section III, and finally those results are summarized in section IV.

II. Methods

A. Generation of H-Bond Configurations. The space group of the *oxygen* lattice in Ice-Ih is $P6_3/mmc$, with 4 oxygen atoms in the unit cell, which can be seen as an oxygen hexagonal close-packed (hcp) structure with half the tetrahedral holes filled likewise by oxygen atoms (a wurtzite structure but with identical atoms). From this lattice orthorombic unit cells with 8 oxygens can be constructed. In this paper we use the orthorombic unit cell as a starting point for which we derive all possible H-bond patterns. The 8-molecule unit cell was not chosen arbitrarily: in the low-temperature domain where the H-bond ordered form of ice Ih (i.e., the ice XI phase) exists, neutron diffraction experiments indicate that the lattice symmetry has been reduced to $Cmc2_1$ [6−9] where the new unit cell is orthorombic with 8 water molecules per unit cell.

[†] Stockholm University.
[‡] Linköping University.

10.1021/jp048434u CCC: $27.50
Published on Web 09/10/2004

The water molecule is situated in a tetrahedral environment. Each water molecule has 6 possible ways of orienting in this environment, if no constraints are applied. For 8 water molecules, the number of possible configurations would thus be $6^8 = 1\,679\,616$. Many of these are forbidden due to Bernal−Fowler ice rules[28] (which, in effect, state that each hydrogen is covalently bound to only one oxygen and H-bonded to only one other oxygen, and that if one water molecule donates an H-bond to another molecule, it cannot accept an H-bond along the same line from that molecule), and after applying these, the remaining number of configurations is 114.

Several of these configurations are related by symmetry operations. After applying mirror, rotation, and translation operators and removing the equivalent patterns, only 16 configurations remain.

The so-obtained configurations were used to generate Cartesian coordinates for the possible O and H positions. We here assumed an ideal orthorombic structure, with the cell dimensions $a = 4.49225$ Å, $b = \sqrt{3}a$, and $c = \sqrt{8/3}a$. This structure was constructed from the ideal oxygen hexagonal close-packed unit cell with a_{hex} axis and c_{hex} axis lengths as above, where the orthorombic lattice vectors are obtained according to $\vec{a} = \vec{a}_{hex} + \vec{b}_{hex}$, $\vec{b} = \vec{b}_{hex} - \vec{a}_{hex}$, and $\vec{c} = \vec{c}_{hex}$. The $c/a = \sqrt{8/3}$ ratio in the ideal hcp structure leads to a nearest-neighbor O(hcp)−O(tetrahedral hole) distance of $\sqrt{3/8}a = 2.7509$ Å.

For comparison, neutron diffraction experiments for ice XI[8] gave that $a = 4.465(3)$ Å and the distortion of the cell lengths from the ideal $P6_3/mmc$ symmetry of the other cell axes were +0.125 Å for the *b*-axis and as little as +0.001 Å for the *c*-axis. In the same study the cell dimensions obtained for untransformed ice Ih were $a = 4.4974(1)$ Å and $c = 7.3236(1)$ Å, which correspond to a nonideal distortion of the *c*-axis by −0.021 Å.

In our idealized structures, the hydrogen atoms were placed in such a way that the internal geometry of each water molecule was 0.9572 Å and 104.52°, which corresponds to that of a water molecule in the gas phase.[29]

The density of our idealized structures are 0.933 g/cm^3, to be compared to the experimental ice XI density 0.930 g/cm^3.[6]

Note that the cell dimensions, i.e., cell axes and angles, were subsequently allowed to relax in the geometry optimizations presented below, with the exception of one of the quantum-chemical methods where analytical cell-size optimizations were not implemented.

B. Quantum-Chemical Methods. The lattice energies of the 16 unit cells were calculated by two different types of quantum-chemical density-functional theory (DFT)[30] computations. In the first DFT approach, the program CASTEP[31] and its implementation of the PW91[32] generalized gradient approximation (GGA) functional together with ultrasoft pseudopotentials[33] and a plane-wave basis set was used.

Full geometry optimizations were performed, for all the intramolecular, intermolecular, and cell dimension degrees of freedom. For comparative purposes (see below) we also made optimizations of only atomic coordinates, keeping the cell dimension at their ideal values.

In the second DFT approach, calculations were done using the BLYP[34,35] functional and the atom-centered numerical basis set (split-valence plus polarization functions) DNP in the DMol3 program.[36] However, optimizations of the cell dimensions were not possible in that code; hence only optimizations of atomic coordinates for the ideal unit cell shape were performed.

Very strict computational conditions were employed. In the CASTEP calculations, a *k*-point spacing of 0.05 Å^{-1} (corresponding to 23 *k*-points) was used to evaluate the energies. The plane wave energy cutoff was 450 eV. During the geometry optimizations, the *k*-point spacing was 0.06 (about 15 k-points) and the plane-wave energy 380 eV ("precise" basis in CASTEP terminology). Optimizations were performed for the coordinates and cell dimensions expressed in the crystallographic space group symmetry. The optimization convergence criterea were root-mean-square gradients being smaller than 0.05 eV/Å and energy difference and displacements between cycles being less than 10^{-5} eV/atom and 0.001 Å, or tighter. The energy of the so obtained structure was then evaluated with the stricter basis and *k*-point sampling, and with the cell transformed back to the original *P*1 (no symmetry) cell, to make sure that the structures were treated equally.

For the DMol3 calculations, energies were evaluated with hexadecapole multipolar expansion of the charge density and the "fine" numerical integration grid, whereas during the optimizations an octupole expansion was used. The optimization convergence criterea were for the energy 10^{-5} hartree, the gradient 0.001 hartree/bohr and the displacements 0.001 bohr, or better.

Our copy of the DMol3 code (version 3.8) did not employ *k*-point sampling, so instead an extended unit cell was used in the periodic calculations. The extended unit cell was obtained by doubling the shortest orthorombic cell axis (the *a*-axis in the original designation). The extended cell (without imposing symmetry) was used when the energies were evaluated, whereas the original *P*1 8-molecule cell (without symmetry) was used during the optimizations.

The lattice energies were calculated by subtracting the water monomer energy from the total potential energy of the unit cell divided by the number of water molecules in the cell. Thus our lattice energies carries a negative sign; i.e., the larger the negative value of the lattice energy, the more stable the structure.

For the unoptimized cell the energy (evaluated with the appropriate DFT method) of a water molecule with the experimental gas-phase geometry (0.9572 Å, 104.52°[29]) was used as reference. For the evaluation of optimized lattice energies, the energy of a geometry-optimized free water molecule was used as reference. The energy-minimum structure of an isolated water molecule using CASTEP/PW91 was 0.9530 Å and 107.01°, and using DMol3/BLYP 0.9728 Å and 104.32°. In CASTEP, which is a pure periodic-DFT code, the energy of the "isolated" water molecule was actually calculated as the energy of a single water molecule in a periodic box with side length 10 Å. This will influence the magnitude of the lattice energy: the total energy of the monomer calculated in a box with side length 15 Å is 0.08 kcal/mol higher than the energy when the side length is 10 Å. However, this is irrelevant for the discussion in the present paper, because we are interested in the relative energy differences between different H-bond polymorphs, and not the absolute magnitudes.

C. Force-Field Models. The lattice energies of the different polymorphs were also calculated using molecular-mechanics analytical potential models for the water−water intermolecular interaction energies and intramolecular deformation energies. We present results using the flexible SPC[37] and COMPASS[38−40] potential models. Many other pair-potential models were also studied, e.g., TIP3P[41] and CVFF[42] but were found to give very similar results to those above when relative energies are considered, which is why they are not reported here.

Optimizations of cell size, cell shape, and atom coordinates were performed to find the energy-minimum structures. Ewald summation[43] with metallic thin-foil boundary conditions was

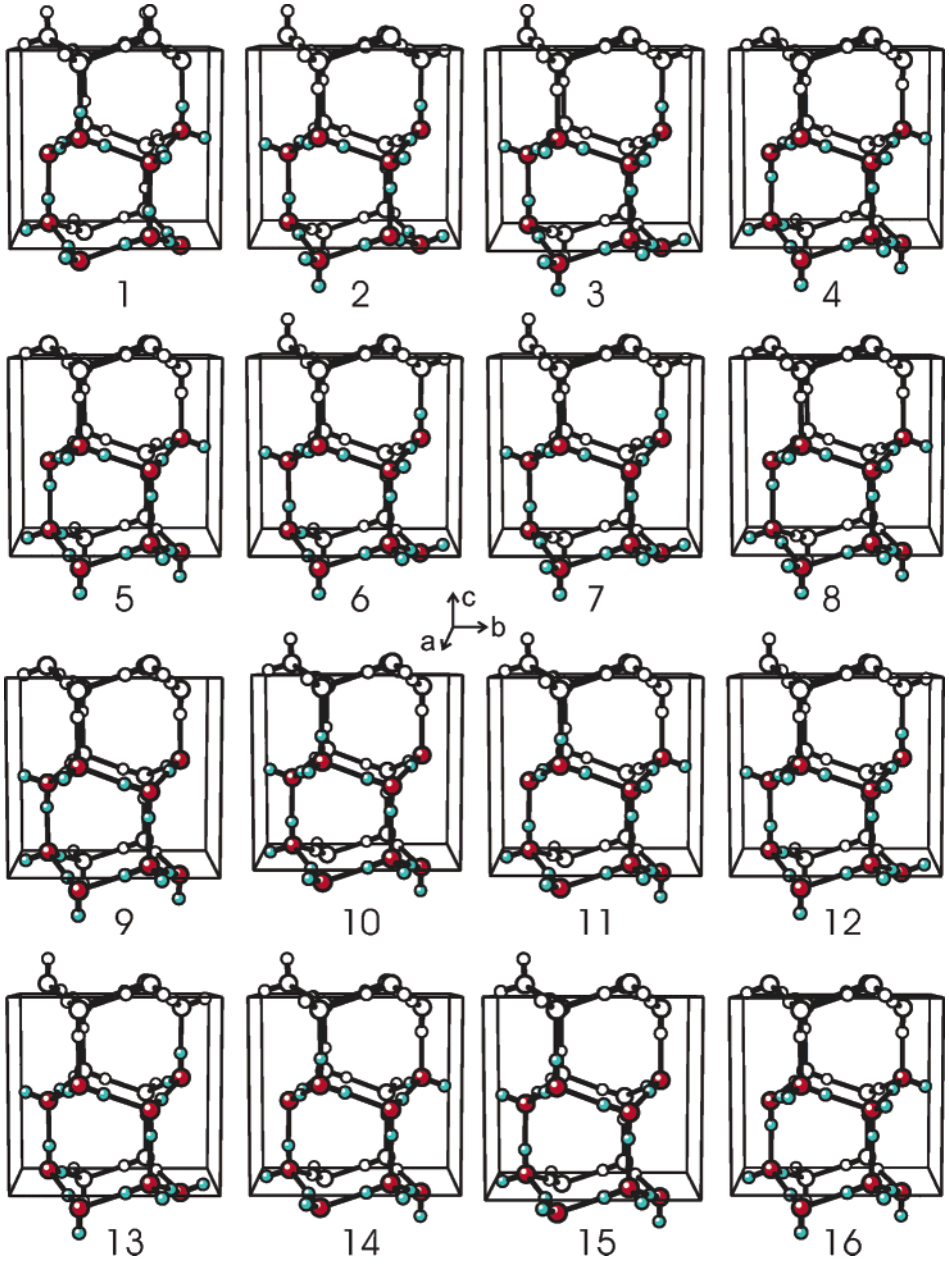

Figure 1. 16 different unique H-bond ordering schemes possible in a 8-molecule orthorombic unit cell. The shaded molecules are the eight molecules in the unit cell, whereas the unshaded molecules are periodic images of the fore mentioned molecules.

used to account for long-range electrostatic interactions. In the SPC code, explicit direct summation out to 6 nearest neighbor cells was performed to account for the nonCoulombic interactions. Computations were performed for COMPASS using the Cerius2[40] program, and for SPC using our own code developed for this purpose.

The energy-minimum structure of a free water molecule using COMPASS is 0.9572 Å and 104.52°, and using flexible SPC 1.000 Å and 109.47°.

III. Results

A. Structures. The 16 final derived symmetry-unique ideal structures can be seen in Figure 1 and the corresponding crystallographic space groups, cell dimensions, and coordinates can be found in Table 1.[44]

Structure no. 1 is the structure suggested by experiment for proton-ordered ice Ih, ice XI, of $Cmc2_1$ symmetry.[9] Structure no. 2 is the structure that early on was suggested by Morokuma and Davidson[14,15] from ab initio-parametrized model-potential lattice-energy considerations to be the most stable, the $Pna2_1$ structure.

Because two of the cells are centered (no. 1 and no. 8), they can be described by smaller primitive hexagonal cells containing 4 water molecules.

Most of the structures possess at least some symmetry. Only one structure is of $P1$ symmetry, no. 16. Howe[16] obtained 17 different structures in his study of the possible ordered structures of ice, two of which belonged to the $P1$ space group. In the present study we also initially obtained two $P1$ structures. But the two structures were found to be enantiomers, and thus chemically equivalent, so only one of these structures needs to be considered in the following. This agrees with the Monto-Carlo study by Buch et al.[25] where 16 different lattice energies were found.

B. Quantum-Chemical and Force-Field Calculations. *1. Lattice Energies.* The energies of the unoptimized structures

TABLE 1: Fractional Coordinates and Cell Dimensions for the 16 Different Proton-Ordered Ice Ih Ideal (Unoptimized) Structures in the Crystallographic Unit Cells, after Transformation from the *P*1 Orthorombic 8-Molecule Cells

	O	H1	H2
1. $Cmc2_1$	4.49225, 7.78080, 7.33581, 90.0, 90.0, 90.0		
	0.0000, 0.3333, 0.5625	0.0000, 0.4510, 0.5244	0.0000, 0.3386, 0.6929
	0.5000, 0.1667, 0.4375	0.6685, 0.2282, 0.4836	
2. $Pna2_1$	7.33581, 7.78080, 4.49225, 90.0, 90.0, 90.0		
	0.5625, 0.9167, 0.5000	0.5164, 0.9702, 0.3235	0.5164, 0.8017, 0.4920
	0.5625, 0.4167, 0.0000	0.6929, 0.4193, 0.0080	0.5244, 0.4755, 0.1765
3. $Pna2_1$	7.33581, 7.78080, 4.49225, 90.0, 90.0, 90.0		
	0.5625, 0.9167, 0.5000	0.5164, 0.9702, 0.6765	0.5164, 0.8017, 0.5080
	0.5625, 0.4167, 0.0000	0.6929, 0.4193, 0.0080	0.5244, 0.4755, 0.1765
4. $Pbn2_1$	4.49225, 7.78080, 7.33581, 90.0, 90.0, 90.0		
	0.5000, 0.8333, 0.5625	0.5080, 0.9483, 0.5164	0.6765, 0.7798, 0.5164
	0.0000, 0.6667, 0.4375	0.0080, 0.6693, 0.3071	0.1765, 0.7255, 0.4756
5. $Pca2_1$	7.78080, 4.49225, 7.33581, 90.0, 90.0, 90.0		
	0.5833, 0.2500, 0.4375	0.5298, 0.0735, 0.4836	0.6983, 0.2420, 0.4836
	0.4167, 0.7500, 0.5625	0.4193, 0.7420, 0.6929	0.4755, 0.5735, 0.5244
6. $P2_12_12_1$	4.49225, 7.78080, 7.33581, 90.0, 90.0, 90.0		
	0.7500, 0.1667, 0.4375	0.5735, 0.2202, 0.4836	0.7420, 0.0517, 0.4836
	0.2500, 0.6667, 0.4375	0.2580, 0.6693, 0.3071	0.4265, 0.7255, 0.4756
7. $P2_12_12_1$	4.49225, 7.78080, 7.33581, 90.0, 90.0, 90.0		
	0.7500, 0.1667, 0.4375	0.5735, 0.2202, 0.4836	0.7420, 0.0517, 0.4836
	0.2500, 0.6667, 0.4375	0.2420, 0.6693, 0.3071	0.0735, 0.7255, 0.4756
8. *C*1*c*1	4.49225, 7.78080, 7.33581, 90.0, 90.0, 90.0		
	0.0000, 0.3333, 0.5625	0.1765, 0.2798, 0.5164	0.0080, 0.4483, 0.5164
	0.5000, 0.1667, 0.4375	0.5080, 0.1693, 0.3071	0.6765, 0.2255, 0.4756
9. *P*1*c*1	7.33581, 4.49225, 7.78080, 90.0, 90.0, 90.0		
	0.0625, 0.2500, 0.1667	0.0164, 0.0735, 0.2202	0.0164, 0.2420, 0.0517
	0.5625, 0.2500, 0.8333	0.5164, 0.0815, 0.7719	0.5164, 0.4185, 0.7719
	0.9375, 0.7500, 0.3333	0.8071, 0.7420, 0.3307	0.9756, 0.5735, 0.2745
	0.4375, 0.7500, 0.6667	0.3071, 0.7500, 0.6614	0.4756, 0.7500, 0.5490
10. *P*1*c*1	4.49225, 7.33581, 8.98450, 90.0, 120.0, 90.0		
	0.6667, 0.6875, 0.1667	0.9020, 0.7256, 0.2255	0.6773, 0.5571, 0.1693
	0.3333, 0.1875, 0.8333	0.4563, 0.2336, 0.7798	0.4563, 0.2336, 0.9483
	0.6667, 0.6875, 0.6667	0.8966, 0.7336, 0.7282	0.5596, 0.7336, 0.7282
	0.3333, 0.1875, 0.3333	0.3386, 0.0571, 0.3386	0.4510, 0.2256, 0.4510
11. *P*1*c*1	7.33581, 7.78080, 8.60200, 90.0, 148.52, 90.0		
	0.5625, 0.9167, 0.5000	0.6929, 0.9114, 0.5000	0.5244, 0.7990, 0.5000
	0.0625, 0.5833, 0.5000	0.0084, 0.6983, 0.4920	0.8399, 0.5298, 0.3235
	0.9375, 0.0833, 0.0000	0.8151, 0.0219, 0.8315	0.1521, 0.0219, 0.1685
	0.4375, 0.4167, 0.0000	0.2992, 0.4193, 0.9920	0.2992, 0.4755, 0.8235
12. $P12_11$	7.78080, 4.49225, 7.33581, 90.0, 90.0, 90.0		
	0.5833, 0.5000, 0.0625	0.5298, 0.6765, 0.0164	0.6983, 0.5080, 0.0164
	0.9167, 0.5000, 0.5625	0.9702, 0.6765, 0.5164	0.8017, 0.5080, 0.5164
	0.0833, 0.0000, 0.0625	0.0807, 0.9920, 0.1929	0.0245, 0.8235, 0.0244
	0.4167, 0.0000, 0.5625	0.4193, 0.0080, 0.6929	0.4755, 0.1765, 0.5244
13. $P12_11$	7.78080, 4.49225, 7.33581, 90.0, 90.0, 90.0		
	0.5833, 0.5000, 0.0625	0.5298, 0.6765, 0.0164	0.6983, 0.5080, 0.0164
	0.9167, 0.5000, 0.5625	0.9702, 0.3235, 0.5164	0.8017, 0.4920, 0.5164
	0.0833, 0.0000, 0.0625	0.0807, 0.9920, 0.1929	0.0245, 0.8235, 0.0244
	0.4167, 0.0000, 0.5625	0.4193, 0.9920, 0.6929	0.4755, 0.8235, 0.5244
14. $P12_11$	7.78080, 7.33581, 4.49225, 90.0, 90.0, 90.0		
	0.9167, 0.0625, 0.2500	0.9114, 0.1929, 0.2500	0.7990, 0.0244, 0.2500
	0.5833, 0.5625, 0.2500	0.5298, 0.5164, 0.0735	0.6983, 0.5164, 0.2420
	0.0833, 0.9375, 0.7500	0.0218, 0.9836, 0.9185	0.0218, 0.9836, 0.5815
	0.4167, 0.4375, 0.7500	0.4193, 0.3071, 0.7420	0.4755, 0.4756, 0.5735
15. $P12_11$	4.49225, 7.78080, 7.33581, 90.0, 90.0, 90.0		
	0.2500, 0.8333, 0.6875	0.4265, 0.7745, 0.7256	0.2580, 0.8307, 0.5571
	0.2500, 0.1667, 0.1875	0.0735, 0.2202, 0.2336	0.2420, 0.0517, 0.2336
	0.7500, 0.3333, 0.6875	0.9185, 0.2718, 0.7336	0.5815, 0.2718, 0.7336
	0.7500, 0.6667, 0.1875	0.7500, 0.6614, 0.0571	0.7500, 0.5490, 0.2256
16. *P*1	4.49225, 7.78080, 7.33581, 90.0, 90.0, 90.0		
	0.0000, 0.6667, 0.0625	0.1765, 0.7202, 0.0164	0.0080, 0.5517, 0.0164
	0.0000, 0.3333, 0.5625	0.1765, 0.2798, 0.5164	0.0080, 0.4483, 0.5164
	0.5000, 0.1667, 0.0625	0.3235, 0.2202, 0.0164	0.4920, 0.0517, 0.0164
	0.5000, 0.8333, 0.5625	0.5080, 0.9483, 0.5164	0.6765, 0.7798, 0.5164
	0.5000, 0.8333, 0.9375	0.6765, 0.7745, 0.9756	0.5080, 0.8307, 0.8071
	0.5000, 0.1667, 0.4375	0.5080, 0.1693, 0.3071	0.6765, 0.2255, 0.4756
	0.0000, 0.3333, 0.9375	0.9920, 0.3307, 0.8071	0.8235, 0.2745, 0.9756
	0.0000, 0.6667, 0.4375	0.0080, 0.6693, 0.3071	0.1765, 0.7255, 0.4756

[a] The row preceding the rows with fractional coordinates presents the space group and cell dimensions *a*, *b*, *c*, α, *β*, *γ* (Å and deg) for the unit cell in compliance with the crystallographic standard settings.

using quantum-chemical calculations and model potentials are displayed in Figure 2 and listed in Table 2.

First of all, one notices that the relative energies among the different structures agree very closely for the two quantum-

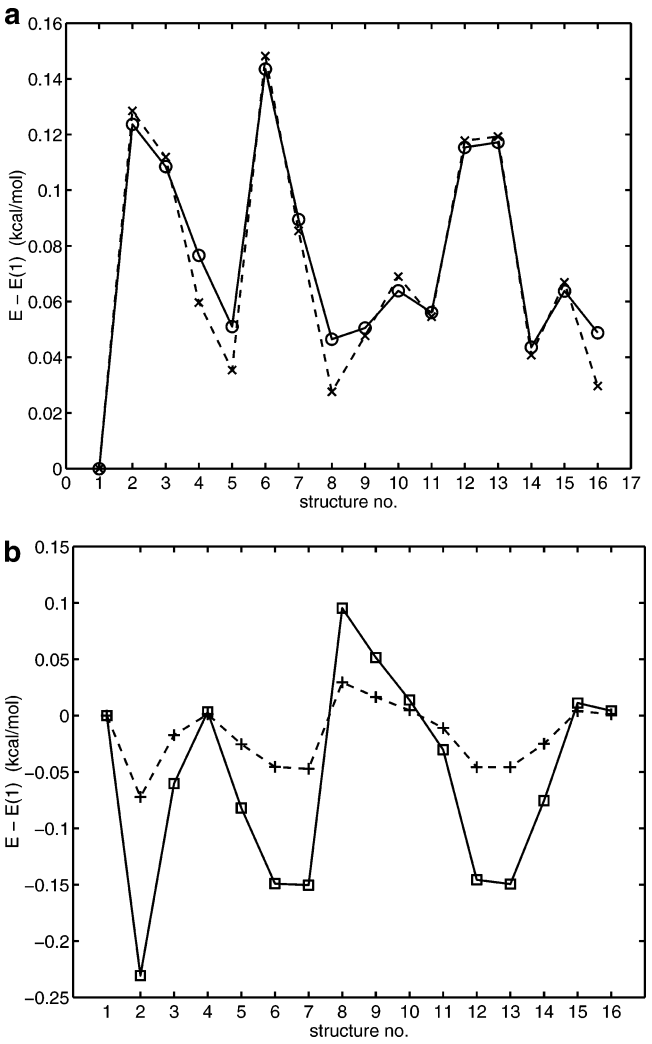

Figure 2. Ideal (unoptimized) cell lattice energies (relative the energy of unit cell no. 1, the $Cmc2_1$ structure) for the 16 unit cells calculated using (a) the DFT methods CASTEP/PW91 (circles) and DMol3/BLYP (crosses) and (b) the force fields COMPASS (squares) and SPC (pluses). Numbering of the unit cells is as in Table 1. The lines connecting the points are intended solely as guidelines for the eye.

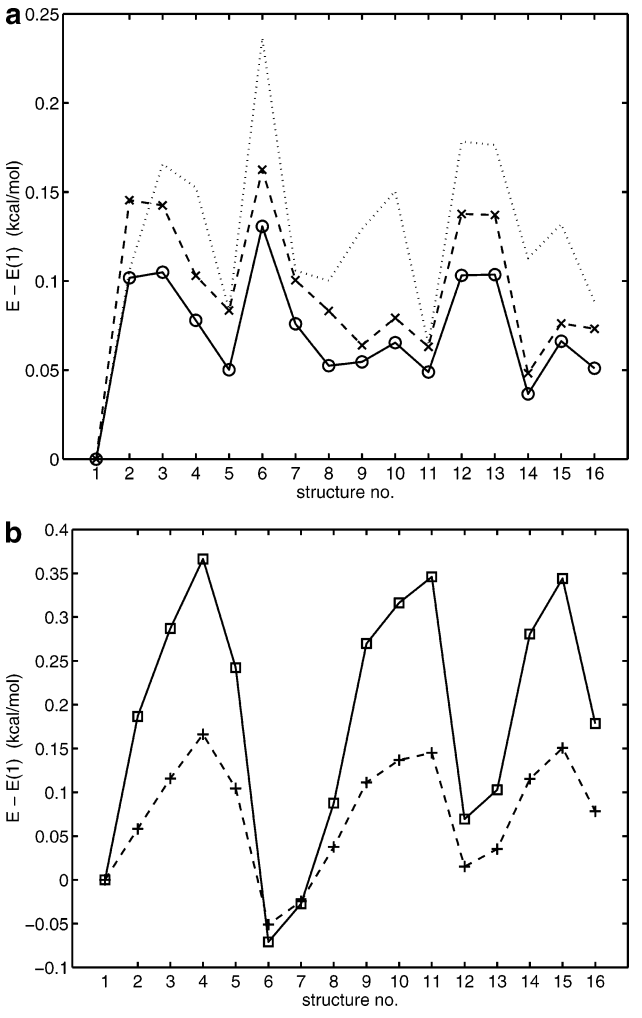

Figure 3. Geometry-optimized cell lattice energies (relative the energy of unit cell no. 1, the $Cmc2_1$ structure) for the 16 unit cells calculated using (a) the DFT methods CASTEP/PW91 coordinate-optimization (circles) and cell size- and coordinate-optimization (dotted line), and DMol3/BLYP coordinate-optimization (crosses) and (b) the force fields COMPASS (squares) and SPC (pluses) cell size- and coordinate-optimization.

chemical computational methods. This could not have been achieved unless very stringent computational conditions had been enforced, i.e., many *k*-points or large unit cells as well as an adequate basis set description.

The quantum-chemical methods both predict the $Cmc2_1$ structure to be lowest in energy, in agreement with the experimental proposed structure for ice XI.[6]

Also the energy results using the model potentials agree well with one another. This is probably due to the similar potential terms from which the potentials were built, because both are flexible two-body potentials and point-charge models.

However, when the quantum-chemical computations and the model potential relative energies for the different polymorphs are compared, little, if any, agreement can be found. The force-field methods erroneously predict the structure no. 2 to be lowest in energy (cf. refs 14 and 15). The reason is likely to be that the potential models are not accurate enough to predict energy differences on the order of tenths of a kilocalorie, which was also noted by Buch et al.[25]

The energies of the geometry-optimized structures can be seen in Figure 3 and Table 2. Also for the geometry-optimized structures, both DFT methods accurately predict the $Cmc2_1$ phase to be lowest in energy.

The quantum-chemical optimized relative energies are still rather similar, when coordinates-only optimization results are considered. The major difference seems to be a difference in the prediction of the energy of structure no. 1, which shifts the graphs relative one another. Displayed in Figure 3b is also the CASTEP cell plus coordinate-optimization energies. These differ a bit more from the abovementioned energies, but still $Cmc2_1$ is lowest in energy, and the difference in energy relative to the next-lowest polymorph is about the same, i.e., 0.06 kcal/mol.

The force-field methods agree with each other also for the optimized structures. But still there is no agreement between quantum-chemical and model potential results.

The experimental lattice energy of ice Ih is −14.1 kcal/mol, if the contributions from intramolecular and intermolecular zero-point vibrational energies are subtracted.[45,46] Table 2 shows that the DMol3/BLYP results are close to the experimental value: e.g., −13.3 kcal/mol for the coordinate-optimized ice no. 1. We analyzed further the performance of the BLYP computations by performing model calculations on a H-bonded water dimer structure, whose geometry was extracted from the BLYP-optimized ice no. 1 structure. The H-bond energy was calculated from the difference between the sum of energies of the two isolated monomers, with internal geometries as in the dimer,

TABLE 2: Lattice Energies (kcal/mol) of the 16 Unique Unit Cells[a]

	CASTEP PW91/pl. wave			DMol BLYP/DNP		COMPASS		flex. SPC	
no.	ideal	optd coo	optd coo + cel	ideal	optd coo	ideal	optd coo + cel	ideal	optd coo + cel
1	−15.50	−16.19	−16.40	−12.05	−13.34	−11.14	−12.57	−13.37	−14.54
2	−15.38	−16.09	−16.30	−11.92	−13.19	−11.37	−12.38	−13.44	−14.48
3	−15.39	−16.08	−16.24	−11.94	−13.19	−11.20	−12.28	−13.39	−14.42
4	−15.43	−16.11	−16.25	−11.99	−13.23	−11.14	−12.20	−13.37	−14.37
5	−15.45	−16.14	−16.32	−12.02	−13.25	−11.22	−12.33	−13.40	−14.44
6	−15.36	−16.06	−16.17	−11.90	−13.17	−11.29	−12.64	−13.42	−14.59
7	−15.41	−16.11	−16.30	−11.97	−13.24	−11.29	−12.60	−13.42	−14.56
8	−15.46	−16.13	−16.30	−12.02	−13.25	−11.05	−12.48	−13.34	−14.50
9	−15.45	−16.13	−16.27	−12.00	−13.27	−11.09	−12.30	−13.36	−14.43
10	−15.44	−16.12	−16.25	−11.98	−13.26	−11.13	−12.25	−13.37	−14.40
11	−15.45	−16.14	−16.34	−12.00	−13.27	−11.17	−12.23	−13.38	−14.40
12	−15.39	−16.08	−16.22	−11.93	−13.20	−11.29	−12.50	−13.42	−14.53
13	−15.39	−16.08	−16.23	−11.93	−13.20	−11.29	−12.47	−13.42	−14.51
14	−15.46	−16.15	−16.29	−12.01	−13.29	−11.22	−12.29	−13.40	−14.43
15	−15.44	−16.12	−16.27	−11.99	−13.26	−11.13	−12.23	−13.37	−14.39
16	−15.45	−16.14	−16.31	−12.02	−13.26	−11.14	−12.39	−13.37	−14.46

[a] Unoptimized (ideal) and optimized structures. CASTEP/PW91, DMol3/BLYP, COMPASS, and SPC calculations. Note that for CASTEP two sets of optimized energies are given: the first refers to optimization of only the atomic coordinates, and the second to joint optimization of coordinates and cell dimensions.

TABLE 3: Optimized Cell Dimensions (Å and deg), the Mean Nearest-Neighbor Oxygen Distances (Å), the Mean Intramolecular OH Bond Lengths (Å) and HOH Angles (deg) from the CASTEP/PW91 Calculations[a]

no.	*a*	*b*	*c*	α	*β*	*γ*	*R*(OO)	*r*(OH)	θ_{HOH}
1	4.380	7.617	7.207	90.00	90.00	90.00	2.692(2)	0.992(1)	108.2(4)
2	4.390	7.657	7.190	90.00	90.00	90.00	2.695(5)	0.992(1)	108.6(1)
3	4.433	7.648	7.171	90.00	90.00	90.00	2.701(5)	0.991(1)	108.2(8)
4	4.442	7.633	7.212	90.00	90.00	90.00	2.706(2)	0.991(0)	107.5(3)
5	4.440	7.593	7.216	90.00	90.00	90.00	2.699(6)	0.991(1)	108.9(1)
6	4.440	7.672	7.251	90.00	90.00	90.00	2.717(3)	0.991(0)	107.7(4)
7	4.444	7.628	7.203	90.00	90.00	90.00	2.703(11)	0.991(1)	108.5(5)
8	4.388	7.663	7.276	90.00	89.83	90.00	2.711(4)	0.991(0)	107.8(2)
9	4.462	7.641	7.221	89.81	90.00	90.00	2.712(4)	0.990(1)	107.7(3)
10	4.460	7.645	7.265	90.00	90.00	88.80	2.719(5)	0.990(1)	108.2(2)
11	4.400	7.617	7.223	90.00	89.18	90.00	2.703(5)	0.991(0)	108.2(1)
12	4.415	7.646	7.242	90.21	90.00	90.00	2.709(7)	0.991(1)	108.2(4)
13	4.414	7.651	7.244	90.12	90.00	90.00	2.708(5)	0.991(1)	107.8(6)
14	4.484	7.622	7.219	90.00	90.00	90.47	2.710(2)	0.990(1)	108.1(2)
15	4.412	7.646	7.242	90.00	89.98	90.00	2.702(11)	0.991(1)	107.7(3)
16	4.421	7.614	7.215	89.93	89.69	89.89	2.700(3)	0.992(1)	108.2(7)

[a] The numbers within parantheses are the standard deviations calculated over all molecules in the particular structure. The cell has been transformed back from the crystallographic unit cell to resemble the original orthorombic 8-molecule unit cell.

and the energy of the dimer. The BLYP functional in combination with the DNP basis set gives an H-bond energy of 4.8 kcal/mol. When instead BLYP with a near-Hartree−Fock limit basis set (aug-cc-pVQZ[47]) is used the H-bond energy is 4.1 kcal/mol (in this calculation the Gaussian03 program[48] was utilized). This implies that the DNP basis-set limitations should result in an overestimation of the H-bond energy. On the other hand, BLYP is not an exact functional. If higher level ab initio theory such as the coupled cluster CCSD(T) method[49] with the aug-cc-pVQZ basis set is used, the resulting (and best estimate) of the H-bond energy is 5.2 kcal/mol, which is higher than the BLYP result with the same basis set. The shortcomings of the BLYP functional itself would thus imply an underestimation of the H-bond energy. The functional and DNP basis-set limitations act in opposite directions, and the two effects cancel to a large extent. (It is interesting to note that the DNP numerical basis set performs better than two common split-valence plus polarization function Gaussian basis sets: the BLYP H-bond energy with the basis sets 6-31G(d,p)[50] and pVDZ[51] is 7.3 and 8.6 kcal/mol, respectively.) The H-bond energy using CASTEP/PW91 for the same dimer as above is 7.8 kcal/mol (using periodic bondary conditions corresponding to a cubic box with side length 10 Å). This overestimation of the H-bond energy is reflected in the overestimation of the absolute lattice energies from the CASTEP/PW91 calculations.

The spread in energies is about 0.25 kcal/mol for the CASTEP fully optimized structures and 0.14 kcal/mol for the unoptimized. This is significantly less than $3/2RT$ at 0 °C (0.81 kcal/mol), which agrees with the observed proton disorder in ordinary ice. The energy difference 0.06 kcal/mol needed to excite the system from the lowest to the first-excited system-energy level is at 20 K comparable to $^3/_2RT$. This energy difference is of the same order of magnitude as the estimation (from the experimental ice Ih residual entropy $\Delta S = 0.81$ cal/(mol K), ref 2) of ΔU for orientational order−proton disorder of 0.06 kcal/mol.[25]

2. Lattice Structures. The CASTEP-optimized cell dimensions and the mean nearest-neighbor oxygen distances are shown in Table 3. The cell dimensions are still similar after the energy-minimization. The intramolecular O−O distances as well as the water molecule internal geometries do not differ significantly between the different structures. Nor are the differences large within a given structure, as can be inferred from the standard deviations.

The parameters α and *γ* in ref 9 measure the deviation of the oxygen atoms from perfect hexagonal symmetry along the *b*-axis and the *c*-axis. Basically, they correspond to an

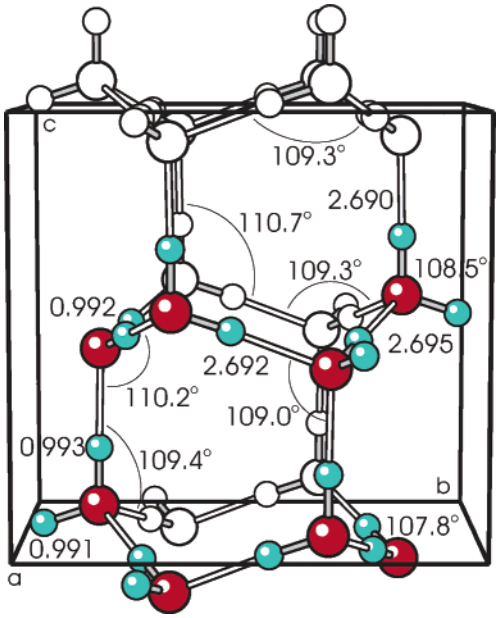

Figure 4. Structure no. 1 ($Cmc2_1$, ice XI) obtained from CASTEP/PW91 energy minimization.

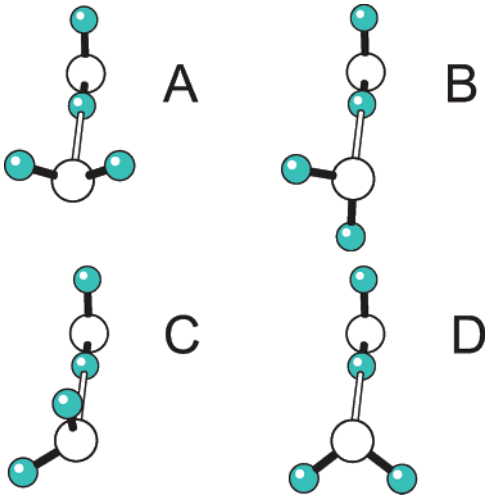

Figure 5. H-bonded dimer configurations in ice Ih, A (or *h-cis*), B (*h-trans*), C (*c-cis*) and D (*c-trans*).

opposite relative translation of the chair ring sheets by an amount $\alpha\vec{b}$ and a puckering of the rings by $\gamma\vec{c}$. When evaluated for this structure the values $\alpha = 0.0025$ and $\gamma = 0.0009$ are obtained. This is considerably smaller than the experimental values $\alpha = 0.02$ and $\gamma = 0.005$[9] or $\alpha = 0.008$.[7]

3. Relation between Structural Characteristics and Energies. The H-bonded water molecule pairs in ice Ih can have four different conformations, as imposed by the tetrahedral H-bond environment in an hexagonal framework of each molecule. These conformations are shown in Figure 5 where the different H-bond types are labeled A, B, C, and D, following the notation by Wong and Whalley.[52] These were labeled as *h-cis*, *h-trans*, *c-cis*, and *c-trans*, respective, in ref 25. Note that due to the hexagonal symmetry of the oxygen lattice, H-bonds within the sheets of chair-conformation six-membered rings transverse to the *c*-axis must be of either A or B type, where the H-bonds running parallel to the *c*-axis must be of C or D type.

The number of the different H-bond types that are present in each of the orthorombic unit cells is listed in Table 4.

It has been suggested that the different conformntions correspond to H-bond classes of different strengths in ice

TABLE 4: Number of *A*, *B*, *C*, and *D* Hydrogen Bond-Dimer Types in the 16 Orthorombic Unit Cells

no.	space group	*A*	*B*	*C*	*D*
1	$Cmc2_1$	12	0	0	4
2	$Pna2_1$	0	12	0	4
3	$Pna2_1$	4	8	4	0
4	$Pbn2_1$	8	4	4	0
5	$Pca2_1$	8	4	0	4
6	$P2_12_12_1$	0	12	4	0
7	$P2_12_12_1$	4	8	0	4
8	$C1c1$	12	0	4	0
9	$P1c1$	10	2	4	0
10	$P1c1$	8	4	4	0
11	$P1c1$	8	4	2	2
12	$P12_11$	2	10	2	2
13	$P12_11$	2	10	2	2
14	$P12_11$	8	4	0	4
15	$P12_11$	8	4	4	0
16	$P1$	10	2	2	2

Ih,[14,15,53−55] where B and D, due to the more favorable orientation of protons from a Coloumb and Van der Waal repulsion point of view in each dimer, should belong to the stronger H-bond class. However, this suggestion is controversial, both from an experimental[56] and a computational[25] point of view.

In their investigations of energies of ice unit cells using analytical potentials, Buch et al.[25] noticed a close linear relationship between the lattice energy and the sum of B and D pairs. In Figure 5 the energy versus the sum of B and D pairs are plotted for the COMPASS potential and for the CASTEP calculation results. For the unoptimized structures (Figure 5a) one can see that such a relationship seems to exist. (It is noteworthy that the COMPASS and CASTEP/PW91 calculations exhibit opposite trends.)

However, when one instead studies the optimized structures (Figure 5b), the correlation between energy and sum of B and D pairs is basically nonexistent (this also applies for the other potentials we have studied). In ref 25 similar observations were made for several force fields, although the correlation usually did not completely disappear (for a polarizable potential model the correlation could be removed if the position of the polarizability center was modified).

In this paper we advocate a different method: fitting the energy to a linear combination, rather than a sum, of the number of B and D pairs. (Because in the unit cells the sum of the number of A and B pairs is always 12, and C and D pairs always 4, only two parameters are necessary.)

In Figure 6a the unoptimized CASTEP/PW91 energies together with a linear expression in terms of number of B (n_B) and number of D (n_D) pairs fitted to these energies are displayed (the dashed line). The equation of the fit is $E_{fit} = 0.0342 + 0.0093n_B - 0.0051n_D$. (Note that the number of B and the number of D pairs enter the expression with opposite signs: large n_B increases and large n_D decreases the lattice energy.)

A very good fit to the unoptimized energies is obtained by fitting only three coefficients. Even more interestingly, if instead the linear expression in n_B and n_D is fitted to the lattice energies of *only the first 3 structures* (the dotted line in Figure 7a) the agreement with the DFT lattice energies of the remaining 13 ices remains very good (the formula now is $E_{fit} = 0.0260 + 0.0092n_B - 0.0069n_D$).

The correlation of the energy with the linear combination of number of B and the number of D pairs is valid to a large extent also for the optimized structures, as can be seen in Figure 7b. The linear equation if fitted to 16 lattice energies is here $E_{fit} = 0.1036 + 0.0099n_B - 0.0196n_D$ and if fitted to

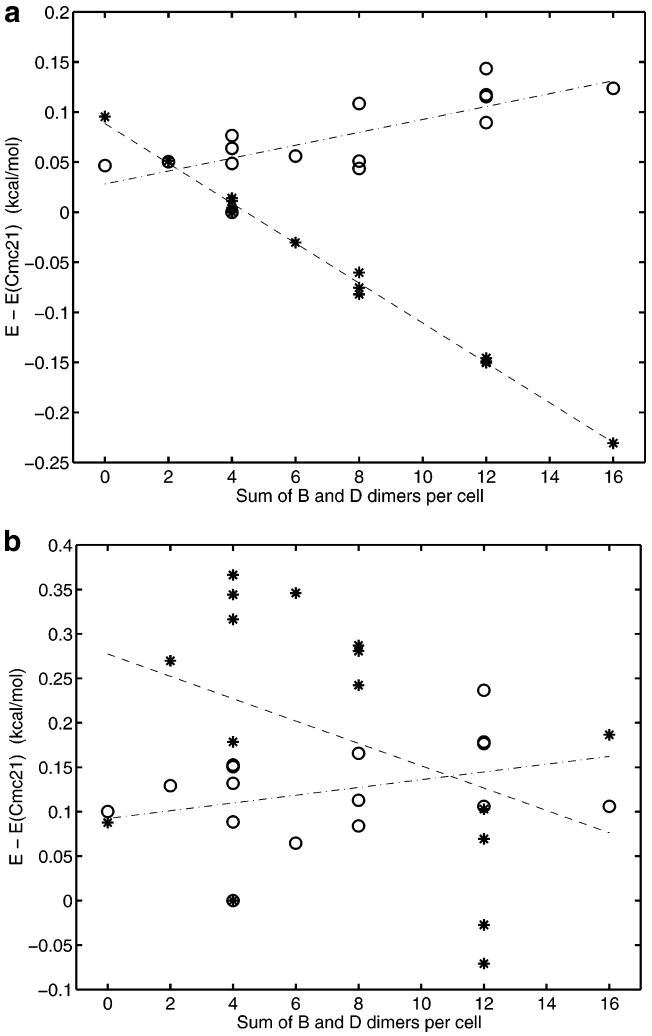

Figure 6. Lattice energy versus the sum of the number of D and B dimer pairs in the 16 different structures: CASTEP/PW91 (circles) and COMPASS calculations (stars); (a) unoptimized (ideal) structures and (b) optimized structures.

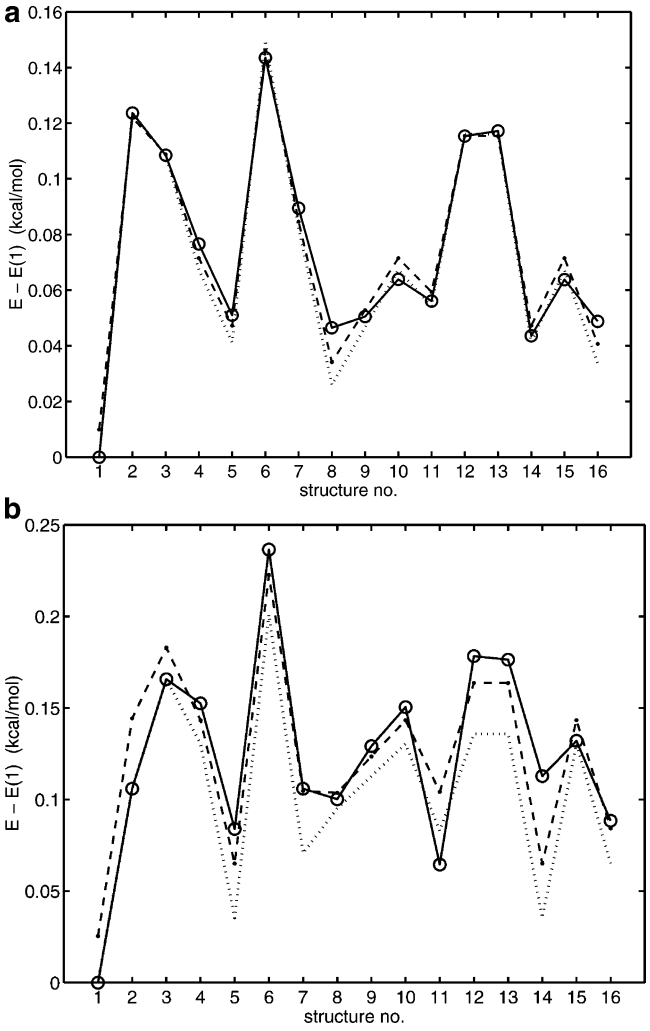

Figure 7. CASTEP/PW91 lattice energies versus a fit to a linear combination of the number of B and the number of D dimer pairs in the 16 different structures: DFT calculations (circles), the fit to the 16 lattice energies (dashed line), and a fit to the lattice energies of only the first three structures (dotted line): (a) unoptimized (ideal) structures and (b) optimized structures.

the first 3 energies $E_{\mathrm{fit}} = 0.0951 + 0.0088n_{\mathrm{B}} - 0.0238n_{\mathrm{D}}$. The fit is slightly worse than for the unoptimized energies, but this is possibly due to flaws in the optimization procedure, such as varying success of convergence.

This type of expression thus appears to have significant predictive power for the stability of different proton-ordered ice Ih structures.

In Figure 8, all the O−O distances in the different ice polymorphs have been plotted, as obtained from CASTEP/PW91 and COMPASS calculations. There is no clear trend to be observed regarding in-chair rings and between chair rings distances, or between the A, B, C, and D types. This contradicts the notion of the existence of strong and weak H-bond classes, if a correlation between H-bond strength and H-bond distance is assumed.[57]

IV. Conclusions

The quantum-chemical calculations using PW91-plane waves and BLYP-localized basis sets, respectively, agree well with each other when relative energies of the different ice polymorphs are concerned (even though the absolute lattice energy magnitudes differ between the two methods). This is especially apparent for the unoptimized structures, but it is also true for the optimized structures when the same degrees of freedom have been optimized. The model potentials cannot reproduce these results and appear to have no predictive power for energy differences of these magnitudes.

Still, analytical potential models are very useful for studying large complicated systems. Given that many different potential models for water exist and still many are being developed,[25] the potential model approach may eventually prove successful. The present quantum-chemical calculations provide a benchmark for those model potentials.

Knowing how the energy depends on H-bond pattern will, by using statistical mechanics, enable us to map out the thermodynamics of the H-bond network. Given that our calculated lattice energies are accurate enough and that the patterns considered are representative as a random subset of all possible patterns in the infinite-molecule unit cell, it is thereby possible to theoretically predict the temperature of the much-debated order−disorder phase transition in ice Ih. Probably investigations using the quantum-chemical methods with larger unit cells will be required to meet this end. For example, in the eight-molecule unit cells, no six-membered rings with a H-bond pattern where each water molecule donates a hydrogen bond to the ring neighbor in a circular pattern (a "head-to-tails" arrangement) are possible. Thus it is clear that possibly important

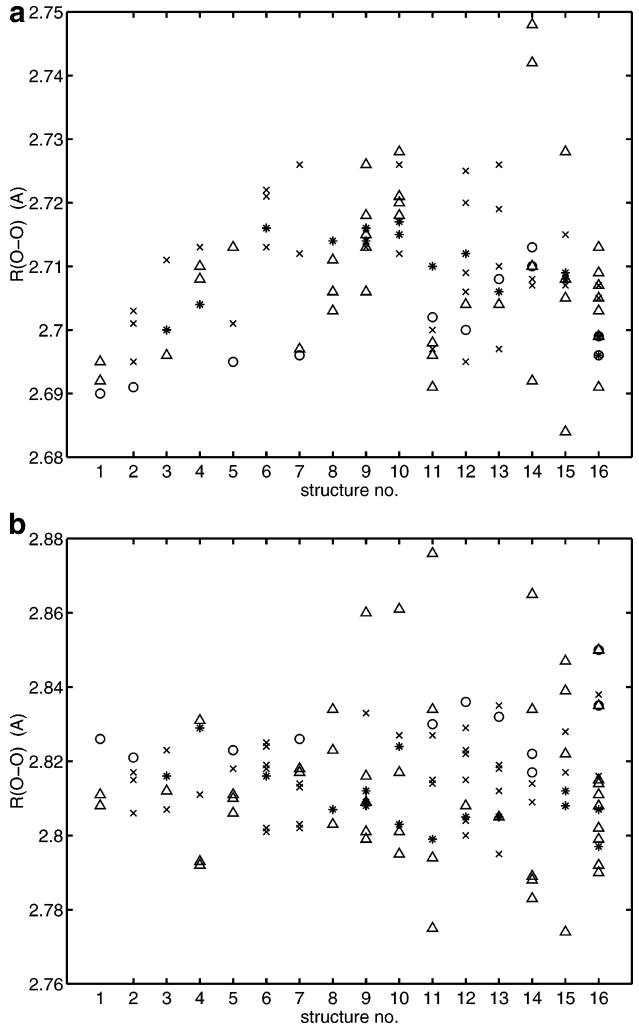

Figure 8. Nearest-neighbor oxygen−oxygen distances in the 16 unit cells, classified according to A (diamonds), B (crosses), C (stars), and D (circles) dimer types: (a) CASTEP/PW91; (b) COMPASS calculations.

structure types have been neglected. Studies of larger unit cells are under way.

Acknowledgment. This research was supported by the Swedish Natural Science Council (VR), by the Swedish Royal Academy of Sciences, and by grants of computer resources from the Swedish National Supercomputer Center (SNAC).

Supporting Information Available: Text files containing Cartesian coordinates for the 16 unoptimized ice structures and cell data for the CASTEP/PW91 optimized structures. This material is available free of charge via the Internet at http://pubs.acs.org.

References and Notes

(1) Eisenberg, D.; Kauzmann, W. *The Structure and Properties of Water*; Oxford: New York, 1969.
(2) Hobbs, P. V. *Ice Physics*; Oxford: New York, 1974.
(3) Pauling, L. *J. Am. Chem. Soc.* **1935**, *57*, 2680
(4) Tajima, Y.; Matsuo, T.; Suga, H. *Nature* **1982**, *299*, 810.
(5) Tajima, Y.; Matsuo, T.; Suga, H. *J. Phys. Chem. Solids* **1984**, *45*, 1135.
(6) Leadbetter, A. J.; Ward, R. C.; Clark, J. W.; Tucker, P. A.; Matsuo, T.; Suga, H. *J. Chem. Phys.* **1985**, *82*, 424.
(7) Howe, R.; Whitworth, R. W. *J. Chem. Phys.* **1989**, *90*, 4450.
(8) Line, C. M. B.; Whitworth, R. W. *J. Chem. Phys.* **1996**, *104*, 10008.
(9) Jackson, S. M.; Nield, V. M.; Whitworth, R. W.; Oguro, M.; Wilson, C. C. *J. Phys. Chem. B* **1997**, *101*, 6142.
(10) Fukazawa, H.; Mae, S.; Ikeda, S.; Watanabe, O. *Chem. Phys. Lett.* **1998**, *294*, 554.
(11) Wang, Y.; Li, J. C.; Kolesnikov, A. I.; Parker, S.; Johnsen, S. J. *Physica B* **2000**, *276*−*278*, 282.
(12) Fortes, A. D.; Wood, I. G.; Grigoriev, D.; Alfredsson; M.; Kipfstuhl, S.; Knight, K. S.; Smith, R. I. *J. Chem. Phys.* **2004**, *120*, 11376.
(13) Morse, M. D.; Rice, S. A. *J. Chem. Phys.* **1982**, *76*, 650.
(14) Davidson, E. R.; Morokuma, K. *J. Chem. Phys.* **1984**, *81*, 3741.
(15) Yoon, B. J.; Morokuma, K.; Davidson, E. R. *J. Chem. Phys.* **1985**, *83*, 1223.
(16) Howe, R. *J. Phys.* **1987**, *C1*(3), 599.
(17) Tse, J. S. *J. Chem. Phys.* **1992**, *9*, 5482.
(18) Barkema, G. T.; de Boer, J. *J. Chem. Phys.* **1993**, *99*, 2059.
(19) Hermansson, K.; Ojamäe, L. *Solid State Ionics* **1995**, *77*, 34.
(20) Pisani, C.; Casassa, S.; Ugliengo, P. *Chem. Phys. Lett.* **1996**, *253*, 201. Casassa, S.; Ugliengo, P.; Pisani, C. *J. Chem. Phys.* **1997**, *106*, 8030.
(21) Hayward, J. A.; Reimers, J. R. *J. Chem. Phys.* **1997**, *106*, 1518.
(22) Morrison, L.; Li, J.-C.; Jenkins, S.; Xantheas, S. S.; Payne, M. C. *J. Phys. Chem. B* **1997**, *101*, 6146.
(23) Hamann, D. R. *Phys. Rev. B* **1997**, *55*, R10157.
(24) Lekner, J. *Physica B* **1998**, *252*, 149.
(25) Buch, V.; Sandler, P.; Sadlej, J. *J. Phys. Chem. B* **1998**, *102*(44), 8641.
(26) Kuo, J.-L.; Coe, J. V.; Singer, S. J.; Band, Y. B.; Ojamäe, L. *J. Chem. Phys.* **2001**, *114*, 2527.
(27) Kuo, J.-L.; Singer, S. J. *Phys. Rev. E* **2003**, *67*, 016114.
(28) Bernal, J. D.; Fowler, R. H. *J. Chem. Phys.* **1993**, *1*(8), 515.
(29) Benedict, W. S.; Gailar, N.; Plyler, E. K. *J. Chem. Phys.* **1956**, *24*, 1139.
(30) Parr, R. G.; Yang, W. *Density Functional Theory of Atoms and Molecules*; Clarendon Press: Oxford, U.K., 1989.
(31) Milman, V.; Winkler, B.; White, J. A.; Pickard, C. J.; Payne, M. C.; Akhmatskaya, E. V.; Nobes, R. H. *Int. J. Quantum Chem.* **2000**, *77*, 895; Accelrys Inc., CASTEP Users Guide, San Diego: Accelrys Inc., 2001.
(32) Perdew, J. P.; Wang, Y. *Phys. Rev. B* **1992**, *46*, 6671. White, J. A.; Bird, D. M. *Phys. Rev. B* **1994**, *50*, 4954.
(33) Version 7.2.1 of the H and O ultrasoft pseudopotentials in the CASTEP program library.
(34) Becke, A. D. *Phys. Rev.* **1988**, *38*, 3098.
(35) Lee, C.; Yang, W.; Parr, R. G. *Phys. Rev. B* **1988**, *37*, 785.
(36) Delley, B. *J. Chem. Phys.* **1990**, *92*, 508.
(37) Toukan, K.; Rahman, A. *Phys. Rev. B* **1985**, *31*, 2643.
(38) Sun, H. *J. Phys. Chem. B* **1998**, *102*, 7338.
(39) Peng, Z.; Ewig, C. S.; Hwang, M.-J.; Waldman, M.; Hagler, A. T. *J. Phys. Chem. A* **1997**, *101*, 7243.
(40) Cerius2, version 3.8, Molecular Simulations Inc., 1998, and version 4.2.1, Accelrys Inc., 2001.
(41) Jorgensen, W. L.; Chandrasekhar, J.; Madura, J. D.; Impey, R. W.; Klein, M. L. *J. Chem. Phys.* **1983**, *79*, 926.
(42) Lifson, S.; Hagler, A. T.; Dauber, P. *J. Am. Chem. Soc.* **1979**, *101*, 5111.
(43) Ewald, P. P. *Ann. Phys.* **1921**, *64*, 253.
(44) The geometry-optimized coordinates can be obtained on request from the corresponding author, e-mail: lars@ifm.liu.se.
(45) Whalley, E. *J. Glaciol.* **1978**, *21*, 13.
(46) Whalley, E. *J. Chem. Phys.* **1984**, *81*, 4087.
(47) Dunning, T. H., Jr. *J. Chem. Phys.* **1989**, *90*, 1007.
(48) Frisch, M. J.; Trucks, G. W.; Schlegel, H. B.; Scuseria, G. E.; Robb, M. A.; Cheeseman, J. R.; Montgomery, J. A., Jr.; Vreven, T.; Kudin, K. N.; Burant, J. C.; Millam, J. M.; Iyengar, S. S.; Tomasi, J.; Barone, V.; Mennucci, B.; Cossi, M.; Scalmani, G.; Rega, N.; Petersson, G. A.; Nakatsuji, H.; Hada, M.; Ehara, M.; Toyota, K.; Fukuda, R.; Hasegawa, J.; Ishida, M.; Nakajima, T.; Honda, Y.; Kitao, O.; Nakai, H.; Klene, M.; Li, X.; Knox, J. E.; Hratchian, H. P.; Cross, J. B.; Adamo, C.; Jaramillo, J.; Gomperts, R.; Stratmann, R. E.; Yazyev, O.; Austin, A. J.; Cammi, R.; Pomelli, C.; Ochterski, J. W.; Ayala, P. Y.; Morokuma, K.; Voth, G. A.; Salvador, P.; Dannenberg, J. J.; Zakrzewski, V. G.; Dapprich, S.; Daniels, A. D.; Strain, M. C.; Farkas, O.; Malick, D. K.; Rabuck, A. D.; Raghavachari, K.; Foresman, J. B.; Ortiz, J. V.; Cui, Q.; Baboul, A. G.; Clifford, S.; Cioslowski, J.; Stefanov, B. B.; Liu, G.; Liashenko, A.; Piskorz, P.; Komaromi, I.; Martin, R. L.; Fox, D. J.; Keith, T.; Al-Laham, M. A.; Peng, C. Y.; Nanayakkara, A.; Challacombe, M.; Gill, P. M. W.; Johnson, B.; Chen, W.; Wong, M. W.; Gonzalez, C.; Pople, J. A. *Gaussian 03*, Revision B.02; Gaussian, Inc.: Pittsburgh, PA, 2003.
(49) Scuseria, G. E.; Schaefer, H. F., III. *J. Chem. Phys.* **1989**, *90*, 3700.
(50) Ditchfield, R.; Hehre, W. J.; Pople, J. A. *J. Chem. Phys.* **1971**, *54*, 724.
(51) Woon, D. E.; Dunning, T. H., Jr. *J. Chem. Phys.* **1993**, *98*, 1358.
(52) Wong, P. T. T.; Whalley, E. *J. Chem. Phys.* **1976**, *65*, 829.
(53) Bjerrum, N. *Science* **1952**, *115*, 386.
(54) Pitzer, K. S.; Polissar, J. *J. Am. Chem. Soc.* **1956**, *60*, 1140.
(55) Li, J. C.; Ross, D. K. *Nature* **1993**, *365*, 327.
(56) Tse, J. S.; Klug, D. D. *Phys. Lett.* **1995**, *198*, 464.
(57) Olovsson, I.; Jönsson, P.-G. In *The Hydrogen Bond − Recent Developments in Theory and Experiments*; Schuster, P., Zundel, G., Sandorfy, C., Eds.; North-Holland: Amsterdam, 1976; Vol. II, Chapter 8, p 393.